

Electron-Cloud and Space-Charge Effects in the Fermilab Booster

K.Y. Ng

Fermi National Accelerator Laboratory, P.O. Box 500, Batavia, IL 60510*

Abstract

The stable region of the Fermilab Booster beam in the complex coherent-tune-shift plane appears to have been shifted far away from the origin by its intense space charge making Landau damping appear impossible. Simulations reveal a substantial buildup of electron cloud in the whole Booster ramping cycle, both inside the unshielded combined-function magnets and the beam pipes joining the magnets, whenever the secondary-emission yield (SEY) is larger than ~ 1.6 . The implication of the electron-cloud effects on the space charge and collective instabilities of the beam is investigated.

*Operated by the U.S. Department of Energy, under contract with the Fermi Research Alliance, LLC.

1 Introduction

Assuming tri-Gaussian distribution, the Fermilab Booster has maximum space charge tune shift of $\Delta\nu_{\max}^{\text{spch}} \sim 0.6$ near injection and the incoherent tune spread is shifted quite far away from the coherent tune. We wonder why Landau damping coming from octupoles can be possible, because the tune spread due to the latter can at most amount to ~ 0.05 . This ambiguity can be resolved if there is an electron cloud around the beam intense enough to neutralize part of the space charge effects, but weak enough not to generate unwanted beam instability issues. Other possibility to answer this ambiguity is also discussed.

2 Stability Contours

Following the analytic solution of Métral and Ruggiero, [1] we computed the stability contour of the Fermilab Booster beam including space charge and octupole tune spread. The dashed curve in every plot of Fig. 1 shows the stability contour of having an octupole tune spread of roughly ± 0.05 with space charge totally neglected. The plot is $\mathcal{Re} \Delta\nu_{\text{coh}}$ versus $\mathcal{Im} \Delta\nu_{\text{coh}}$, which is proportional to $-\mathcal{Im} Z_1^\perp$ versus $-\mathcal{Re} Z_1^\perp$ with Z_1^\perp being the transverse impedance experienced by the beam. The region under the contour implies stability while the region above implies instability. When space charge is turned on according to the information in Table I, this stability contour becomes the solid curve shown in Fig. 1(a). Now the stability region becomes much wider as a result of the large space-charge tune spread. Unfortunately, this wide stable area has been shifted far far away from center of the plot as a result of the large incoherent tune shift. Thus the inductive part of the vacuum chamber impedance must be extraordinary large so as to be under the contour in order to stabilize

Table I: Some properties of the Booster and its beam near injection.

Radius R (m)	75.42
Total Energy E (GeV)	1.40
No. of filled rf buckets	81
No. of empty rf buckets	3
Bunch intensity	6×10^{10}
Tune ν_x/ν_y	6.8/6.8
Normalized rms emittance ($10^{-6} \pi\text{m}$)	2.00
Rms bunch length σ_z (m)	0.70

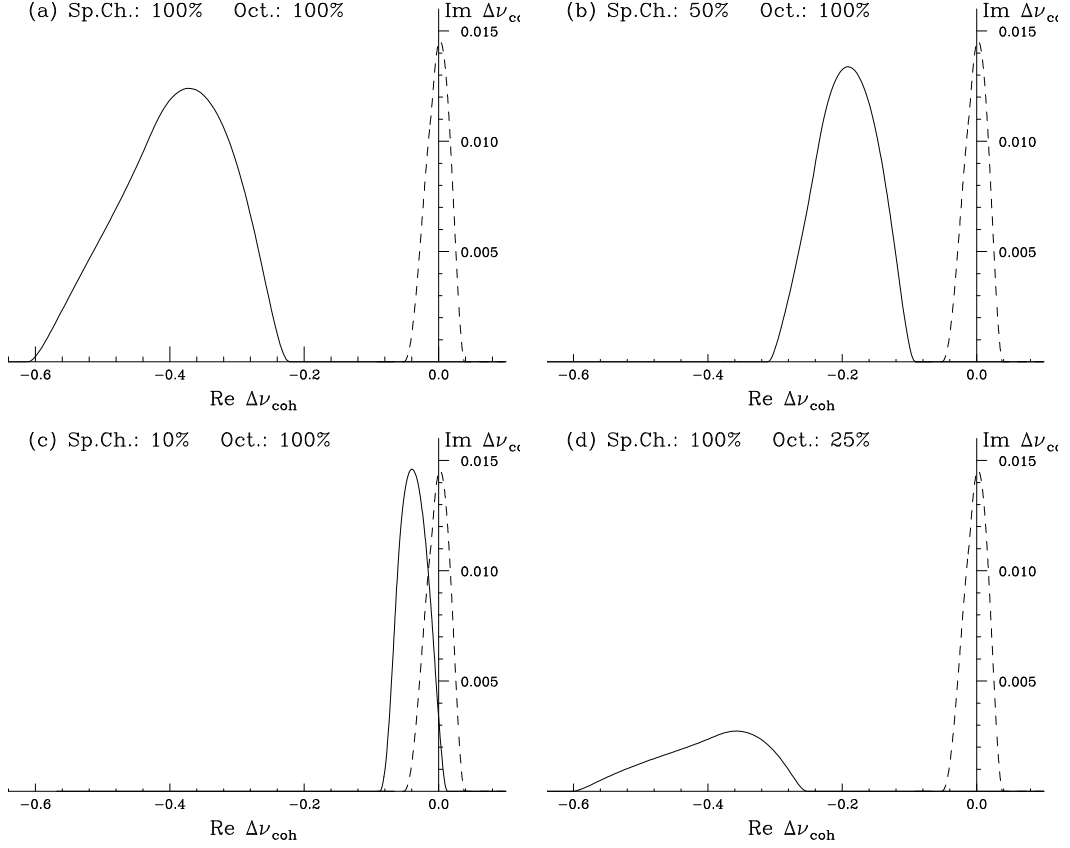


Figure 1: In all plots, stability contour from octupole alone is shown in dashes as reference. (a) The stability contour changes to the solid curve with the introduction of full space charge force. (b) Its spread becomes narrower and the shift from the $\mathcal{I}m \Delta\nu_{\text{coh}}$ -axis is smaller with 50% of space charge, and (c) it even covers the $\mathcal{I}m \Delta\nu_{\text{coh}}$ -axis at 25% capacity. (d) As the octupole current reduces to 25% but with full space charge, the stability contour becomes about 25% tall only.

the beam. Physically, the inductive impedance of the vacuum chamber must be large enough to cancel the space charge impedance, or the tune shift from the inductive impedance must be large enough to cancel that coming from space charge. Unfortunately, the inductive impedance is usually very much smaller than the space charge impedance. In the derivation of the contours, coasting beam has been assumed, but the peak current has been used.

Figure 1(b) shows the situation when the space charge effect is reduced by half. We see as expected that the stability contour becomes narrower and moves closer to the vertical axis. When space charge is reduced to just 10%, we see in Fig. 1(c) that the stability contour now covers the $\mathcal{I}m \Delta\nu_{\text{coh}}$ axis, implying that even with zero or very tiny amount of inductive impedance, the beam will be stable if $|\mathcal{R}e Z_1^\perp|$ is not too large. Physically, this is the situation when the space-charge effect of the beam is small enough and the octupole tune spread stabilizes the beam. Figure 1(d) shows the situation of having space charge in full force but with the octupole current reduced to 25%. Here we see the spread of the stability contour is of roughly the same width as that in Fig. 1(a). However, its height has been reduced to 25%, implying that the stability region has been greatly reduced. It also tells us that the ability of Landau damping comes from the octupole tune spread instead of space charge. In fact, when the octupole current is reduced to zero, the stability contour collapses onto the $\mathcal{R}e \Delta\nu_{\text{coh}}$ axis. Physically, the center of the beam is not affected by the space charge force, which therefore cannot generate any Landau damping by itself.

3 Electron Cloud

The code POSINST [2] is employed to study electron cloud buildup in the Booster. The Booster is made up of 24 unshielded combined-function F-magnets and 24 unshielded combined-function D-magnets. Their cross sections are shown in Fig. 2. In the simulations, the F-magnet is represented by a $13.0'' \times 1.64''$ rectangular pipe with uniform magnetic field 0.084102 Tesla, while the D-magnet is represented by a $12.0'' \times 2.25''$ rectangular pipe with 0.071480 Tesla. According to the observed initial loss rate of $\sim 1.5\%$ for the first 500 turns, beam loss to the surrounding per beam particle per meter is 6.49×10^{-8} , and each of these strayed particles is assumed to generate 100 electrons. These electrons dominate over the electrons generated by collision with ions at the vacuum pressure of 1×10^{-7} Torr. Figure 3 shows the electron density around one transverse $\sigma_{x,y}$ of the beam inside the F- and D-magnets for various secondary-emission yield (SEY). The bunch pattern has been taken to be 81 bunches plus 3 empty buckets. Thus the density dips in the plots correspond to the

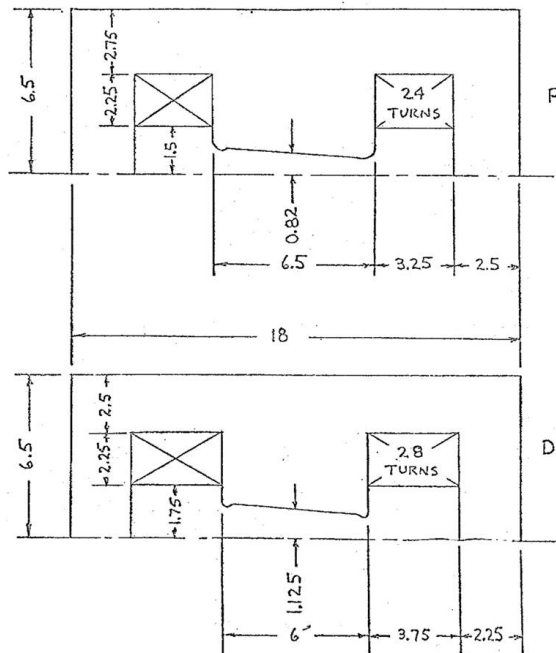


Figure 2: Cross sections of the F- and D-magnets. All dimensions are in inches. The bending fields at the centers are 0.084102 and 0.071480 Tesla, respectively.

ends of revolution turns. We see that saturation is reached in the D-magnet when $SEY \geq 1.5$, while it requires a $SEY \geq 1.9$ to have saturation in the F-magnet. This observation is due to the fact that the vertical gap of the D-magnet is much bigger than that of the F-magnet and can therefore trap more electrons. The same simulations were performed for the circular stainless steel pipes joining the magnets. They consist of 168 m of 2.25" pipe and 28.8 m of 4.25" pipe. The results are shown in Fig. 4. Again the larger pipe appears to have the ability to trap more electrons. In any case, however, electron cloud reaches saturation when $SEY \gtrsim 1.6$.

It is unfortunate that we have no knowledge of the SEY for the unshielded magnet laminations. In below, we try to do the investigation using $SEY=1.6$, implying that electron cloud buildup will saturate in the round pipes and inside the D-magnets, but not necessary in the F-magnets. We next look into the electron density near the beam in Fig. 5. Since the peak beam particle density is given by

$$\rho_b^{\text{pk}} = \frac{N_b}{(2\pi)^{3/2} \sigma_x \sigma_y \sigma_z} = 2.72 \times 10^{14} \text{ m}^{-3}, \quad (3.1)$$

the electron density appears to be very much smaller. However, the particle density decreases very rapidly away from the beam axis, but the electron density does not. The particle density

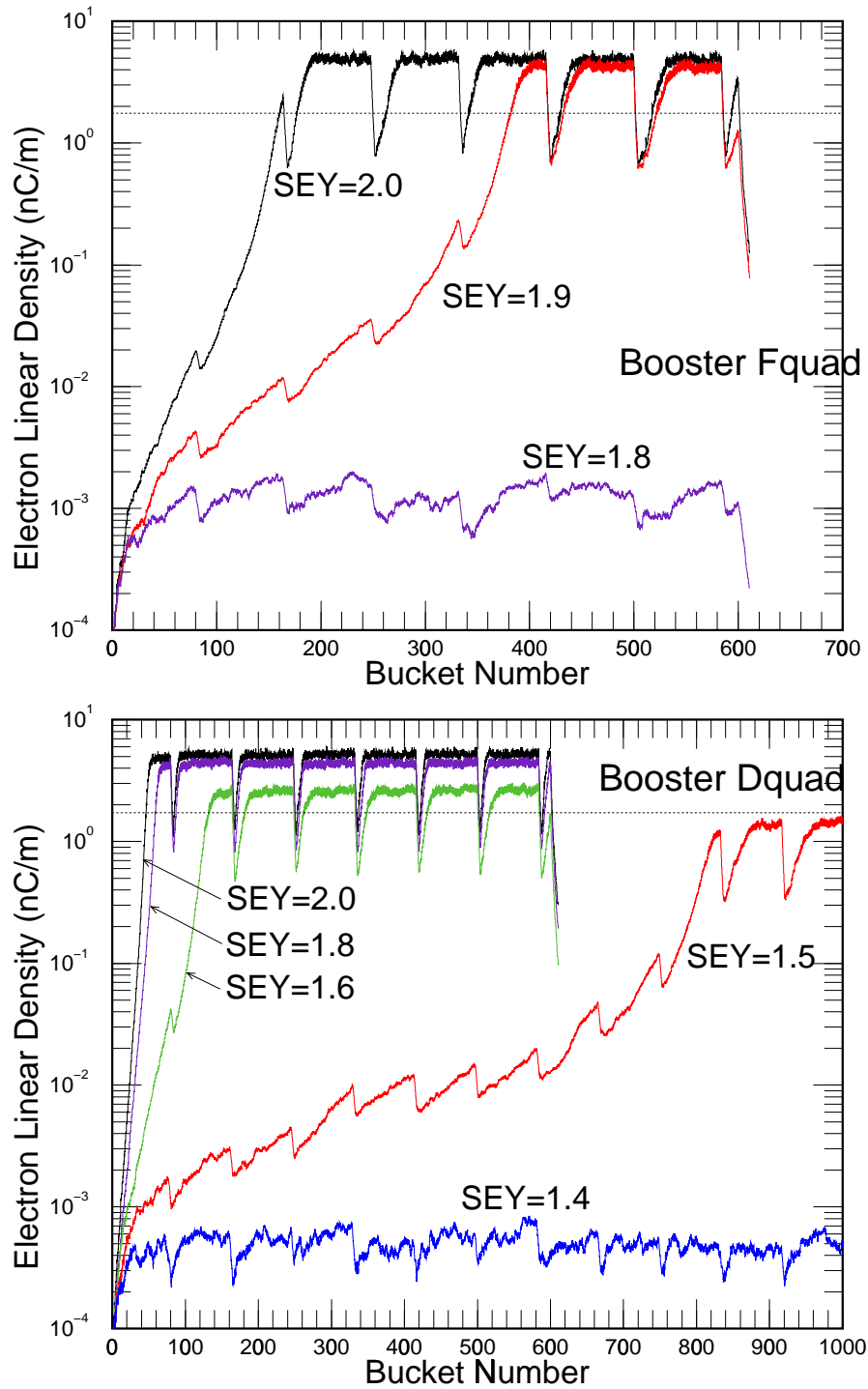


Figure 3: (Color) Electron cloud linear density inside an F-magnet (top) and a D-magnet (bottom) for various values of the secondary-emission yields (SEY). The average linear density of the beam is shown in dashes as a reference.

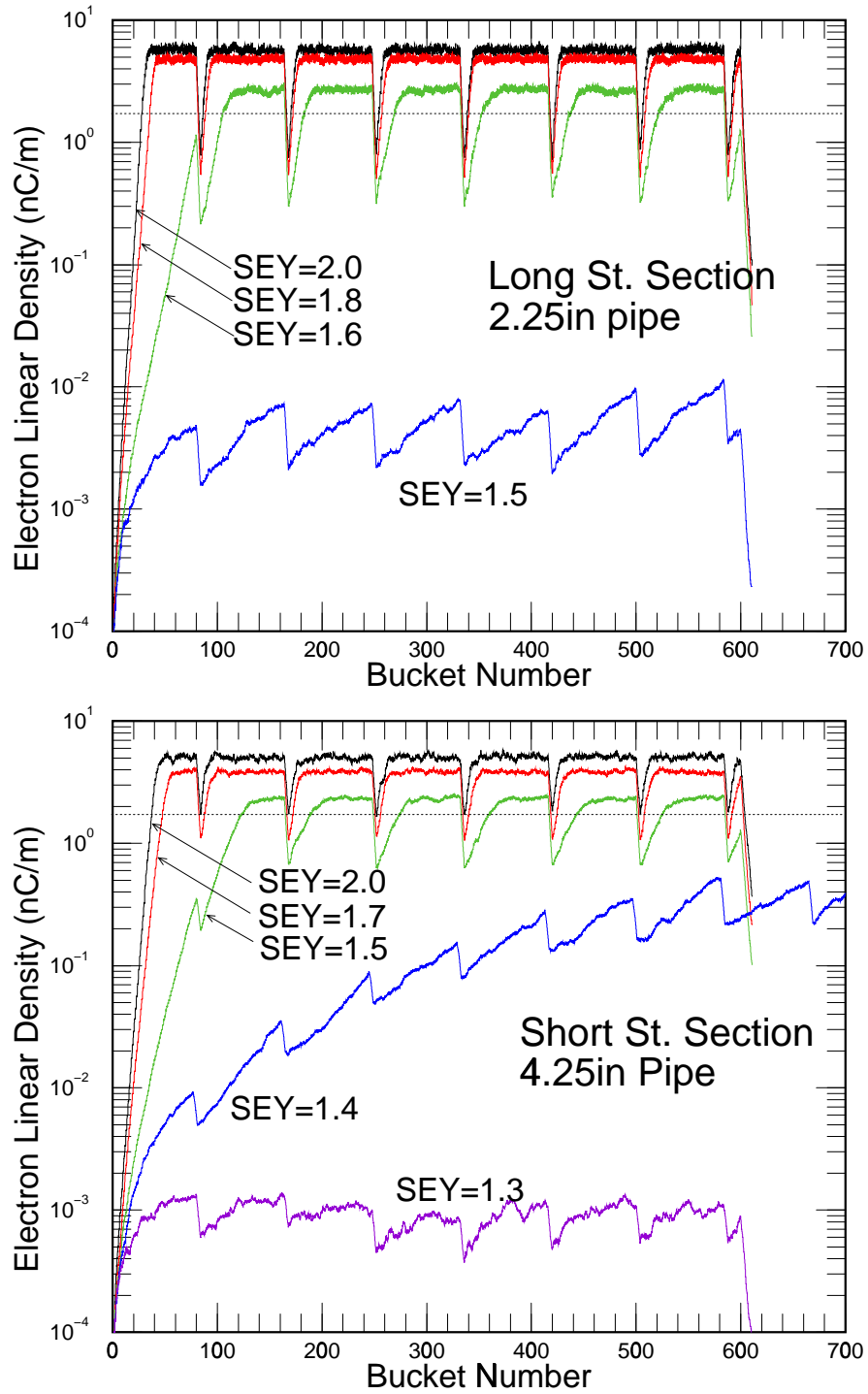


Figure 4: (Color) Electron cloud linear density inside the 2.25'' pipe in the long-straight sections (top) and the same inside the 4.25'' pipe in the short-straight sections (bottom). The average linear density of the beam is shown in dashes as a reference.

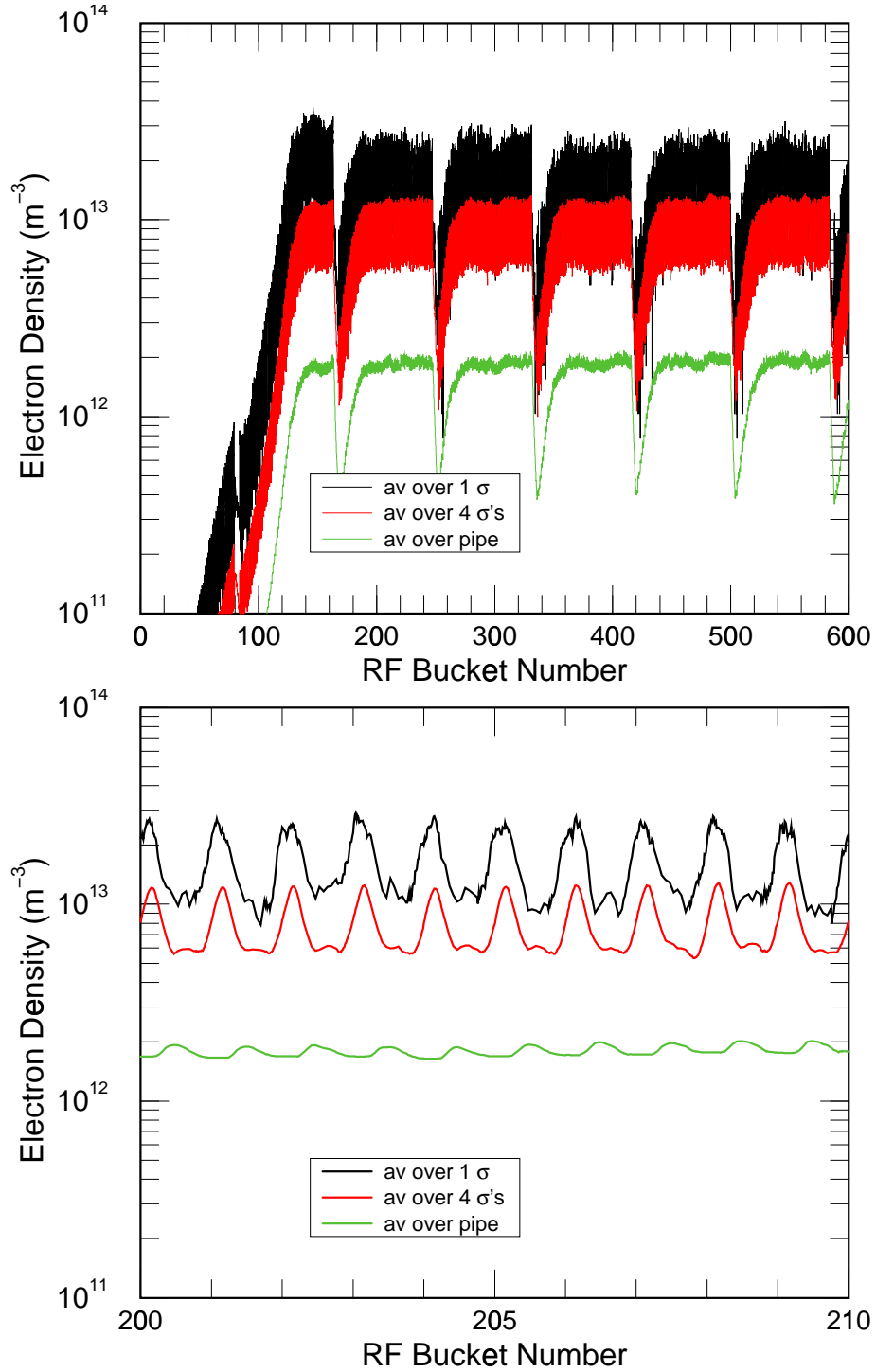


Figure 5: (Color) Electron density inside a D-magnet with $SEY=1.6$, with its zoomed view between rf buckets 200 and 210 shown below. Black curve is the electron density averaged over one $\sigma_{x,y}$ of the beam; red curve is the electron density averaged over four $\sigma_{x,y}$'s of the beam; green curve is the electron density averaged over the whole cross section of the magnet.

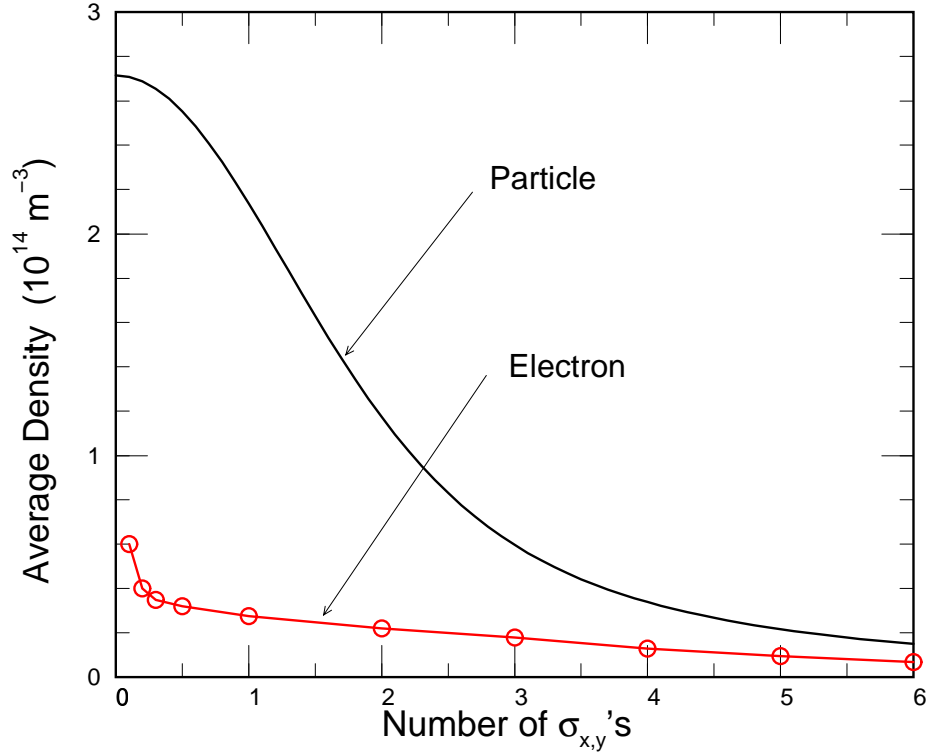


Figure 6: Particle density averaged over $n \sigma_{x,y}$'s is seen to decrease rapidly with n . The corresponding electron density averaged over $n \sigma_{x,y}$'s, although smaller, yet decreases less rapidly.

averaged over $n \sigma_{x,y}$'s is given by

$$\rho_b(n\sigma_{x,y}) = \rho_b^{\text{pk}} \frac{2}{n^2} \left(1 - e^{-n^2/2}\right) \quad (3.2)$$

and is shown in Fig. 6. Alongside, we also plot the corresponding electron density averaged over the same $n \sigma_{x,y}$'s computed using POSINST. For example, the ratio of electron density to particle density averaged over two $\sigma_{x,y}$'s is 0.187. The implication is that the cancellation of space charge of the beam may be $\sim 18.7\%$, which is rather appreciable. The inductive tune shift of the beam particle in the electron cloud, $\Delta\nu_{\text{cl}}$, can also be estimated from the assumption of a uniform electron density [3]

$$\Delta\nu_{\text{cl}} = \frac{\pi\rho_e r_p R^2}{\gamma\beta^2\nu_y}, \quad (3.3)$$

where $r_p = 1.535 \times 10^{-18}$ m is the classical proton radius, and γ and β are the relativistic factors. The beam particles reside mostly within two $\sigma_{x,y}$'s of the bi-Gaussian distribution. We therefore read off $\rho_e = 2.2 \times 10^{13} \text{ m}^{-3}$ from Fig. 6 as the electron density averaged

over two $\sigma_{x,y}$'s. This gives $\Delta\nu_{cl} = 0.11$, which is 18.0% of the maximum space-charge tune shift of $\Delta\nu_{\max}^{\text{spch}} = 0.60$. The tune depression of an intense Booster beam as well as the inductive part of the magnet laminations and connecting beam pipe has been measured and computed. They are found to supply at most an inductive tune shift of ~ 0.04 (see Appendix). Thus, in total, at most $\sim 25\%$ of the space charge will be canceled by electron cloud and inductive walls. As is shown in the stability contours of Fig. 1, there is still no possibility for the transverse impedance of the beam to be inside the stable region. However, as will be suggested below, when we take into account that fact that the beam is bunched instead of coasting, the situation will be much better. Before going into that let us first compute the effective impedance generated by the electron cloud and study its possible effects on collective instabilities of the Booster beam.

4 Collective Instabilities

The effects of the electron cloud can be modeled by a short range wake. In Heifets derivation, [4] this wake is, at a distance z from the source particle,

$$W_1(z) = \frac{8Z_0\rho_e\omega_e R}{(1+p)\lambda_b^{\text{pk}}} W_{\text{eff}}(z), \quad (4.1)$$

where $p = \sigma_y/\sigma_x$ is the aspect ratio of the particle beam with linear density $\lambda_b^{\text{pk}} = N_b/\sqrt{2\pi}\sigma_z$, where σ_z is the rms bunch length. The *effective* wake $W_{\text{eff}}(z)$ is depicted in Fig. 7 for various ratios of the rms spread of the cloud $\Sigma_{x,y}$ to that of the beam $\sigma_{x,y}$. This wake resembles a resonance wake with the resonant frequency near the electron angular bounce frequency ω_e . The transverse impedance can be readily computed by performing a Fourier transform, with the result depicted in Fig. 8,[†] where an average electron density of $\rho_e = 1 \times 10^{13} \text{ m}^{-3}$ in the vicinity of the beam has been assumed. Alongside, we have also plotted the transverse impedance of the 48 laminated magnets. [6] We see that the impedance arising from the electron cloud is mostly dominated by the resonance near the electron bounce frequency and is much larger than that from the magnets below ~ 150 MHz. This is to be expected, because we wish to have a larger inductive impedance at low frequencies to cancel the space charge of the beam more efficiently, and large inductive impedance naturally brings in large resistive impedance. The large impedance will unavoidably bring about severe transverse

[†]A similar figure appears also in Ref. [7], an extract of this paper. There, the right plot of Fig. 4 is incorrect because the electron bounce frequency has been computed with an incorrect formula which is $\sqrt{2}$ too big.

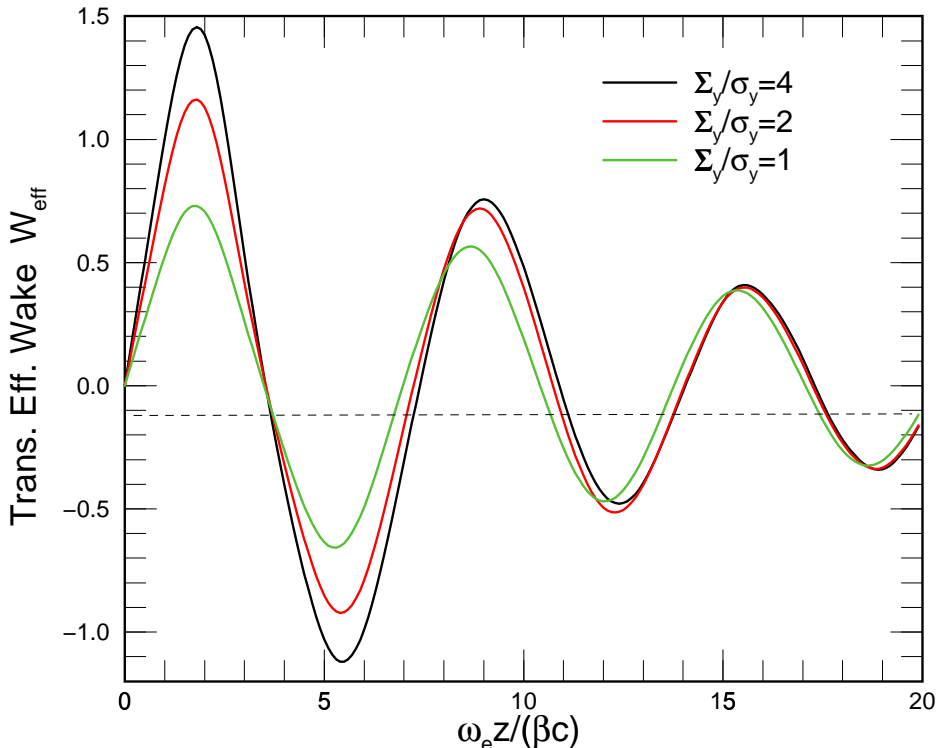


Figure 7: (Color) Effective wake derived from an electron cloud around a round beam, where ω_e is the angular electron bounce frequency while Σ_y and σ_y are the vertical rms radii of the cloud and beam, respectively.

head-tail instabilities and transverse microwave instabilities to the Booster beam. Detailed analysis will be devoted to a separate paper. [5] Since these rather strong instabilities have not been observed, it is possible that the SEYs of the magnet laminations and the adjoining beam pipes are much smaller, for example, $\lesssim 1.3$, so that electron cloud does not accumulate around the beam. For example, the electron cloud effects will become minimal when the cloud density is reduced to below $1 \times 10^{12} \text{ m}^{-3}$.

5 Bunching Effects

In the discussion of stability contour in Sec. 2, a coasting Booster beam has been assumed. The situation of a bunched beam can be different. This is because there will be many more particles, for examples those away from the longitudinal center, having smaller space-charge tune shifts. Since the derivation of the stability contour for a bunched beam is more involved, here we will study instead the simpler problem concerning the distribution

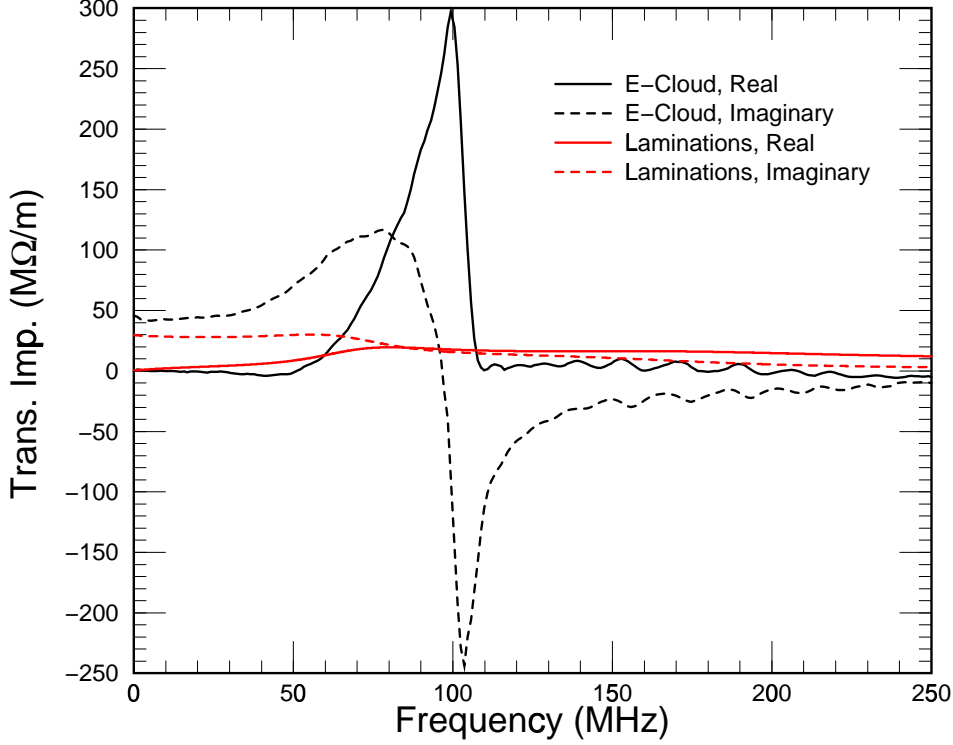


Figure 8: (Color) Real and imaginary parts of the transverse impedances arising from electron cloud in the Booster, which appears to resonate strongly near the electron bounce frequency ω_e . The much smaller transverse impedance coming from the magnet laminations is also shown for comparison.

of space-charge tune shifts of the particles inside a bunch, which can also shed some light on the shape of the stability contour.

The distribution of space-charge tune shift in a coasting beam with circular cross section and bi-Gaussian distributed shows that the distribution is skewed towards higher values, with

$$\frac{\langle \Delta\nu^{\text{spch}} \rangle}{\Delta\nu_{\text{max}}^{\text{spch}}} = 0.6334, \quad \left(\frac{\Delta\nu^{\text{spch}}}{\Delta\nu_{\text{max}}^{\text{spch}}} \right)_{\text{rms}} = 0.1678. \quad (5.1)$$

This distribution, called $f_{2D}(\Delta\nu^{\text{spch}}/\Delta\nu_{\text{max}}^{\text{spch}})$, is shown in dashes in Fig. 9. [8] It also shows that the distribution is essentially zero when $\Delta\nu^{\text{spch}}/\Delta\nu_{\text{max}}^{\text{spch}} < 0.15$. This curve has close resemblance to the stability contour in Fig. 1(a). In fact, they should be closely related. For a bunch, however, the space-charge tune shift distribution can be very different because the particles near the two ends have rather small space-charge tune shifts.

Let the longitudinal or linear distribution of the bunch be $\lambda_b(z)$, which is normalized to

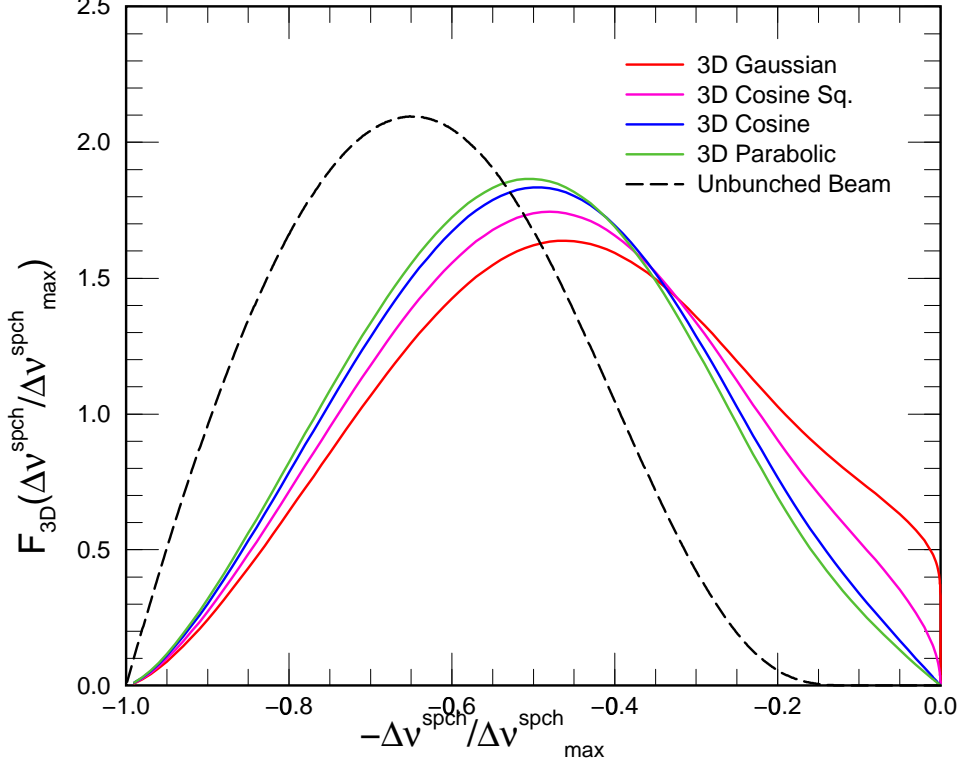


Figure 9: (Color) Plots of distribution in space-charge tune shift in a round bunch with longitudinal Gaussian, cosine square, cosine, and parabolic distribution. The transverse distribution is bi-Gaussian. The distribution of a coasting beam is also shown for comparison.

unity after integrating over z . For a slice of the bunch at z , the number of particles residing in the slice is $N_b \lambda_b(z) dz$. Thus the maximum space-charge tune shift inside this slice is

$$\Delta\nu_{\text{max}}^{\text{spch}}(z) = \Delta\nu_{\text{max}}^{\text{spch}}(0) \frac{\lambda_b(0)}{\lambda_b(z)}. \quad (5.2)$$

Here, $\Delta\nu_{\text{max}}^{\text{spch}}(0)$ is the maximum space-charge tune shift of the whole bunch, and is the same as $\Delta\nu_{\text{max}}^{\text{spch}}$ in Eq. (5.1) for the 2D coasting beam. For simplicity, we set $\Delta\nu_{\text{max}}^{\text{spch}} = 1$ below. Thus for this particular slice, the distribution in space-charge tune shift is

$$F_{\text{slice}}(\Delta\nu^{\text{spch}}, z) = f_{2D} \left(\Delta\nu^{\text{spch}} \frac{\lambda_b(0)}{\lambda_b(z)} \right) \frac{\lambda_b(0)}{\lambda_b(z)}, \quad (5.3)$$

which is properly normalized that an integration over $\Delta\nu^{\text{spch}}$ gives unity. The distribution

for the whole bunch is therefore

$$\begin{aligned} F_{3D}(\Delta\nu^{\text{spch}}) &= \int_{-z}^z F(\Delta\nu^{\text{spch}}, z') \lambda_b(z') dz' \\ &= \int_{-z}^z f_{2D} \left(\Delta\nu^{\text{spch}} \frac{\lambda_b(0)}{\lambda_b(z')} \right) \lambda_b(0) dz', \end{aligned} \quad (5.4)$$

where the limits of integration $\pm z$ are given by the excursion of z' at the maximum space-charge tune shift, or

$$\Delta\nu^{\text{spch}} \frac{\lambda_b(0)}{\lambda_b(z)} = 1. \quad (5.5)$$

Take the Gaussian distribution as an example, the 3D distribution is given by

$$F_{3D}(\Delta\nu^{\text{spch}}) = \int_{-z}^z f_{2D} \left(\Delta\nu^{\text{spch}} e^{z'^2/2} \right) \frac{dz'}{\sqrt{2\pi}}, \quad (5.6)$$

with

$$z = \sqrt{-2 \ln \Delta\nu^{\text{spch}}}. \quad (5.7)$$

For the cosine square distribution,

$$\lambda_b(z) = \frac{1}{\hat{z}} \cos^2 \frac{\pi z}{2\hat{z}}, \quad (5.8)$$

the 3D tune shift distribution is

$$F_{3D}(\Delta\nu^{\text{spch}}) = \int_{-\theta}^{\theta} f_{2D} \left(\frac{\Delta\nu^{\text{spch}}}{\cos^2 \theta'} \right) \frac{2d\theta'}{\pi}, \quad (5.9)$$

with

$$\theta = \cos^{-1} \sqrt{\Delta\nu^{\text{spch}}}. \quad (5.10)$$

For the cosine distribution,

$$\lambda_b(z) = \frac{\pi}{4\hat{z}} \cos \frac{\pi z}{2\hat{z}}, \quad (5.11)$$

the 3D tune shift distribution is

$$F_{3D}(\Delta\nu^{\text{spch}}) = \int_{-\theta}^{\theta} f_{2D} \left(\frac{\Delta\nu^{\text{spch}}}{\cos \theta'} \right) \frac{d\theta'}{2}, \quad (5.12)$$

with

$$\theta = \cos^{-1} \Delta\nu^{\text{spch}}. \quad (5.13)$$

Finally, for the parabolic distribution

$$\lambda_b(z) = \frac{3}{4\hat{z}} \left(1 - \frac{z^2}{\hat{z}^2} \right), \quad (5.14)$$

the 3D tune shift distribution is

$$F_{3D}(\Delta\nu^{\text{spch}}) = \int_{-z}^z f_{2D} \left(\frac{\Delta\nu^{\text{spch}}}{1-z'^2} \right) \frac{3dz'}{4}, \quad (5.15)$$

with

$$z = \sqrt{1 - \Delta\nu^{\text{spch}}}. \quad (5.16)$$

These distributions are shown in Fig. 9. These curves show that there are plenty of particles with space-charge tune shift close to zero tune shift, and they are more plentiful when the longitudinal linear density has longer tails. A longitudinal Gaussian distribution may have been too ideal, but the cosine-square distribution is rather realistic. We expect the stability contour for a bunch behaves similarly. As a result, beam stability can be attained provided that there is some reasonable inductive impedance, some extra tune spread arises from octupoles, and $|\text{Re } Z_1^\perp|$ is not too big, while electron cloud need not play an important role.

6 Conclusion

An analytic solution of the stability contour for the Fermilab Booster has been performed following the derivation of Métral and Ruggiero. Due to the large space-charge tune shift at injection, it appears that the stability region has been shifted by so much that Landau damping will not be possible unless the inductive impedance of the vacuum chamber is extraordinarily large. We have studied the possibility of electron cloud buildup in the Fermilab Booster, hoping that the cloud would cancel at least part of the large space-charge tune shift near injection, so that Landau damping will become possible in the presence of octupoles. We found that at most the cancellation is only about 25%, when a SEY=1.6 is assumed. On the other hand, the electron buildup generates a strong resonant impedance near the electron bounce frequency, which is very much larger than the impedance arising from the magnet laminations. Such a large transverse impedance will drive severe transverse microwave instabilities and head-tail instabilities in the beam. Since such strong transverse instabilities have not been observed, it is possible that the SEY is in fact much less and there is not a significant electron cloud buildup. On the other hand, the effects of electron cloud on collective beam instabilities have not been well understood at this moment. It is possible that the derivation of the wake of the cloud and its subsequent interactions with the particle beam require more detailed investigation.

The analytical model of Métral and Ruggiero assumes a coasting beam. However, the beam of the Booster is bunched. As a result, there are many more low space-charge tune

shifted particles and the tune shift distribution is now skewed back towards the zero tune shift side. We believe the stability contour for a bunched beam will behave in the same way; i.e., there will be ample stable region under the stability contour close to the origin of the complex coherent-tune-shift space. As a result, a small amount of inductive impedance together with some octupole tune spread will be able to stabilize the Booster beam, provided that $|\mathcal{R}e Z_1^\pm|$ is not too large.

Appendix: Tune Depression of Booster

A.1 Measured Tune Depression

Turn-by-turn transverse positions of some Fermilab Booster bunches were measured by Huang [9] for 2-, 4-, 6-, 8-, and 10-turn injection, corresponding to the intensities of 0.92, 1.85, 2.79, 3.69, and 4.66×10^{10} particles per bunch, respectively. A pinger was turned on and its voltage was ramped from 0.6 kV at injection to 3.8 kV near extraction. The pinger was fired every 0.5 ms with 2.0- μ s pulse width, so that the bunches were kicked vertically every 0.5 ms. Each set of data covers 2000 turns or the whole ramping Booster cycle. Each data set is divided into small pieces, each 0.5 ms long (225 to 300 turns), so that the coherent motion induced by each pinger pulse can be analyzed. The data are supplied to an independent-component-analysis routine [9] to solve for the betatron oscillation modes and the vertical betatron tune ν_y is computed from the fast Fourier transform (FFT) of the temporal pattern. The independent-component-analysis routine increases the accuracy of tune measurement since the data of all the beam-position monitors (BPMs) are used.

The vertical betatron tunes throughout the Booster 15-Hz cycle had been measured. However, only those measurements up to the transition time (roughly at 17 ms or 9500 turns) were used for the present analysis. These measurements for all the data sets are plotted in Fig. 10. The tune depressions due to beam intensity are clearly seen at various times. The measurements near turn 3000 were found to come from errors. Near injection, the tune depression of a 10-turn injection beam is roughly 0.03. The 10-turn beam corresponds to a bunch intensity of $N_b = 4.66 \times 10^{10}$. Thus, the tune depression for a $N_b = 6 \times 10^{10}$ beam is ~ 0.04 . The tune depression is also called the *coherent betatron tune shift*.

A.2 Compared with Theoretical Computation

The transverse coupling impedance of the laminated magnets together with the beam pipes joining them has been computed, from which the tune depression can be inferred. Here, we wish to approach the problem in the reverse order by computing the impedance from the measured tune depressions and comparing the result with the theory.

Since the Booster bunches have roughly Gaussian linear distribution, the Sacherer's

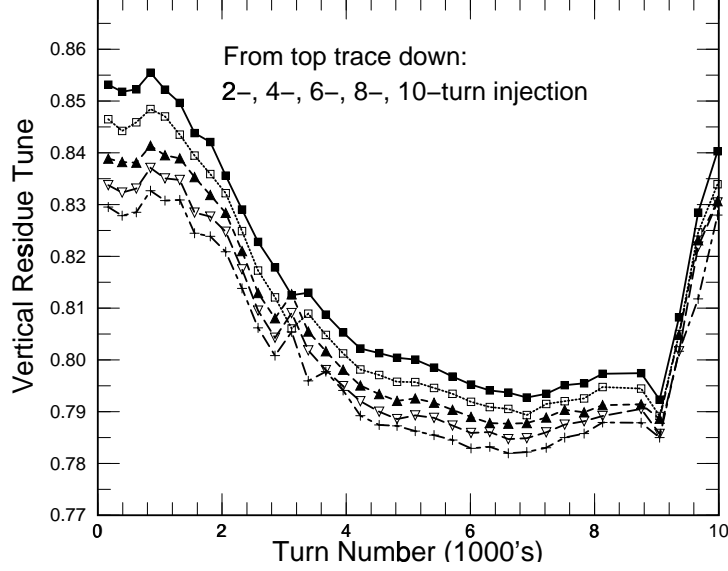


Figure 10: Measured coherent vertical betatron tune shifts in the Fermilab Booster as functions of revolution turn number for 2-, 4-, 6-, 8-, and 10-turn injection, corresponding to intensity of 0.92, 1.85, 2.79, 3.69, and 4.66×10^{10} particles per bunch.

integral equation of transverse motion is solved in the Hermite mode. The lowest order perturbation gives, for the most easily excited rigid-dipole mode ($m = 0$ and $k = 0$), the *dynamic* betatron tune shift[‡]

$$\Delta\nu_y|_{\text{dyn}} = -\frac{e^2 N_b R}{8\pi^{3/2} \beta E_0 \nu_y \sigma_\tau} \mathcal{I}m Z_1^Y \Big|_{\text{eff}}, \quad (\text{A.1})$$

where σ_τ is the rms bunch length and the effective vertical impedance is

$$\mathcal{I}m Z_1^Y \Big|_{\text{eff}} = \frac{\int_{-\infty}^{\infty} \frac{d\omega}{2\pi} \mathcal{I}m Z_1^Y(\omega) e^{-\omega^2 \sigma_\tau^2}}{\int_{-\infty}^{\infty} \frac{d\omega}{2\pi} e^{-\omega^2 \sigma_\tau^2}}. \quad (\text{A.2})$$

In above, a broadband impedance has been assumed so that the summation over the betatron sidebands can be replaced with an integral.

To obtain the coherent betatron tune shift, the incoherent tune shift must be added onto the dynamic tune shift. Thus one should be careful about what should be included in

[‡]If one tries to approximate the betatron tune shift of a bunch by the betatron tune shift of a coasting beam, with the average bunch current replaced by the peak current $I_{\text{pk}} = eN_b/(\sqrt{2\pi}\sigma_\tau)$, the numerical factor in the denominator of Eq. (A.1) changes from $8\pi^{3/2}$ to $4\sqrt{2}\pi^{3/2}$.

the transverse impedance when the coherent betatron tune shift is computed. For example, the transverse space-charge impedance can be expressed as

$$Z_1^V|_{sc} = \frac{Z_0}{\pi\beta^2\gamma^2} \sum_i L_i \left[\frac{\epsilon_{sc}^V}{a_{vi}^2} + \frac{\xi_1^V - \epsilon_1^V}{h_i^2} \right], \quad (\text{A.3})$$

where the summation runs over each section of the vacuum chamber of length L_i , half-height h_i , and half height of the beam a_{vi} , while ϵ_{sc}^V , ξ_1^V , and ϵ_1^V represent the appropriate space-charge coefficients and Laslett's electric image coefficients. [11] Only the terms involving the coherent Laslett's image coefficient ξ_1^V should be included.[§] The beam pipes joining the magnets have such a contribution. The contribution is important at low energy, $\sim 24 \text{ M}\Omega/\text{m}$, but rolls off as $(\beta\gamma)^{-2}$ as the beam energy increases. As for the magnets, this contribution may not be appropriate, because the Laslett's coherent electric coefficient ξ_1^V is for perfectly conducting vacuum chamber only. Here, the laminated magnet pole faces are not perfectly conducting. The modification can be obtained by noticing that the term involving ξ_1^V in Eq. (A.3) can be rewritten as

$$\frac{\xi_1^V}{h_i^2\gamma^2} = \frac{\xi_1^V}{h_i^2} - \beta^2 \frac{\xi_1^V}{h_i^2}, \quad (\text{A.4})$$

where the first term is for the electric image in the perfectly conducting walls of the vacuum chamber and the second term is for the magnetic image in the same perfectly conducting walls. For the laminated magnets, the electric image is formed at the enclosure of the magnet, which carries most of the return current at low frequencies. The magnetic image is formed at the magnetic pole faces. We therefore have instead the replacement

$$\frac{\xi_1^V}{h_i^2\gamma^2} \longrightarrow \frac{\xi_1^V}{\bar{h}_i^2} + \beta^2 \frac{\xi_2^V}{h_i^2}, \quad (\text{A.5})$$

where \bar{h}_i^2 stands for the radius of the magnet enclosure and $\xi_2^V = \pi^2/16$ is the Laslett's coherent magnetic coefficient for two horizontal parallel perfect magnetic surfaces separated by the distant $2h_i$. Attention should also be paid to the change in sign of the magnetic contribution from perfectly conducting surfaces to perfect magnetic surfaces. Since the radius of enclosure is usually much larger than the magnet half gap ($\bar{h}_i^2 \gg h_i^2$), the electric contribution is small and can be neglected. For example, if the enclosure radius is $\bar{h}_i = 8''$, the electric contribution is only $0.4 \text{ M}\Omega/\text{m}$, where $\xi_1^V = \frac{1}{2}$ for a circular enclosure has been

[§]The tune shift corresponding to the self-force part of Eq. (A.3) is cancelled by the incoherent self-force tune shift. The tune shift corresponding to the ϵ_1^V part is cancelled by the incoherent tune shift due to images.

used. Thus the contribution of the magnets to the transverse impedance becomes with the summation going over all the magnets,

$$Z_1^V|_{\text{mag}} = \frac{Z_0 \xi_2^V}{\pi} \sum_i \frac{L_i}{h_i^2}. \quad (\text{A.6})$$

However, more thinking reveals that the above expression is still not quite correct, because the pole surfaces are not exactly perfectly magnetic. They are laminated instead. The effects of the laminations and cracks will become more apparent as the frequency increases. In fact, a somewhat more accurate representation of the transverse impedance of the laminated magnets is the one computed and depicted in Fig. 8, of which the low-frequency limit is just the bypass inductive impedance. The model of laminated magnets employed in the computed result should take care of both terms on the right side of Eq. (A.5). There are other contributions to $\mathcal{I}m Z_1^V$ at low frequencies, such as BPMs, bellows, steps, etc. Since they amount to only $\sim 0.4 \text{ M}\Omega/\text{m}$ up to 200 MHz in the Fermilab Tevatron, [12] it is safe to regard them as negligible compared with the laminated magnets in the Fermilab Booster. In short, the main contributions to the vertical coherent betatron tune shift arise from the bypass inductive impedance of the magnets plus the electric-image contribution of the pipes joining the magnets.

For each of the data piece, Huang performed a linear fit to the measured coherent vertical tune depression as a function of bunch intensity. Then following Eq. (A.1), the coherent part of the effective transverse impedance was computed. The rms bunch lengths were taken from a previous measurement [10] by fitting Gaussians to the linear waveforms of the beam recorded using a wall-gap monitor. As shown in Fig. 11, the bunch length is almost intensity independent up to transition crossing near 17 ms. The resulting effective impedance is plotted as squares in Fig. 12. The exotic point at 3000 turn arises from a measurement error.

For the theory side, the effective vertical dipole impedance is then evaluated according to Eq. (A.2) by including only the impedance computed for the laminated magnets as well as the contribution of the coherent Laslett's image coefficients from the beam pipes joining the magnets. The result, not exactly the same as Ref. [9], is shown as a solid curve in Fig. 12. The agreement is excellent after understanding that the impedance of the laminated magnets displayed in Fig. 8 is only an estimate using the concept of surface impedance and does not evolve rigorously from Maxwell equations. Nevertheless, the experiment appears to reproduce the right order of magnitude for the bypass inductive impedance.

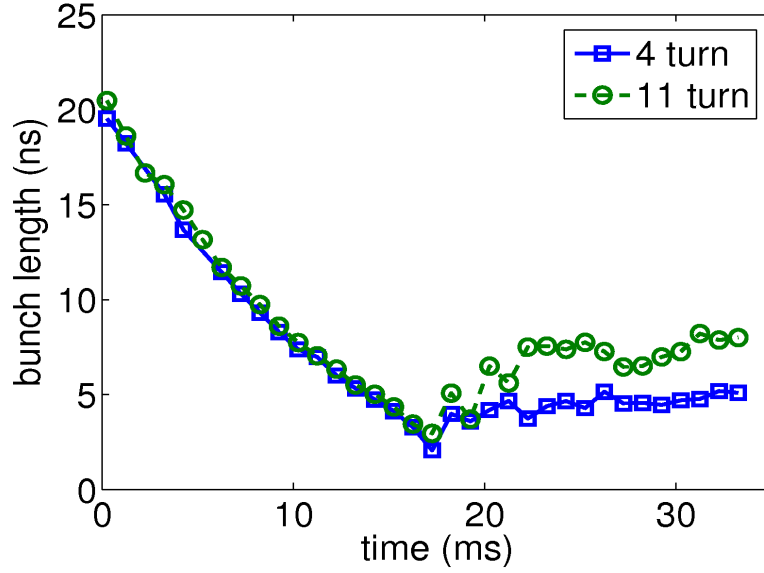


Figure 11: (Color) Rms bunch length measured by Huang by fitting a Gaussian to the waveforms recorded by the wall-gap monitor for 4-turn and 11-turn injection. The measurement was made at 1-ms interval throughout the whole Booster ramping cycle. Transition crossing is at 17.5 ms.

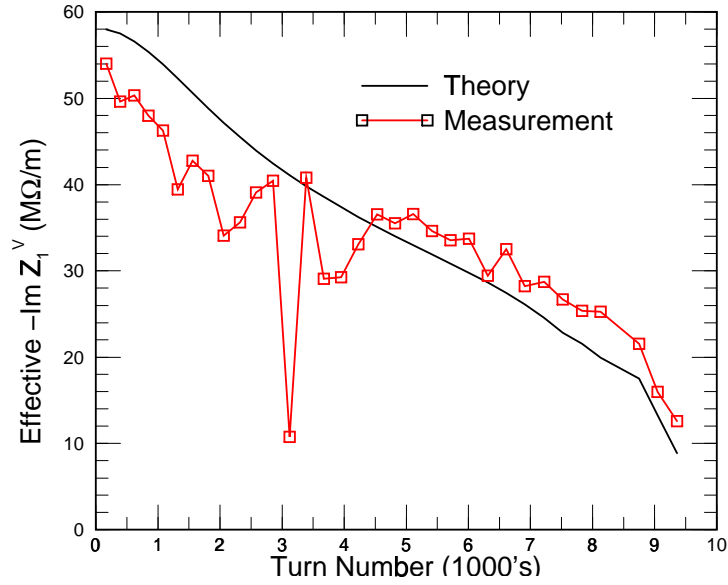


Figure 12: Squares: effective coherent vertical dipole impedance in the Fermilab Booster derived from measured coherent tune shifts. The point near 3000 turns arises from an error in the measurement. Solid curve: the same from evaluating the integrals in Eq. (A.2) using the computed impedance of the laminated magnets and the contribution from the beam pipes joining the magnets.

References

- [1] E. Métral and F. Ruggiero, *Stability diagrams for Landau damping with two-dimensional betatron tune spread from both octupoles and non-linear space charge*, CERN-AB-2004-025 (ABP), 2004.
- [2] M.A. Furman and G.R. Lambertson, *The Electron-Cloud Instability in the Arcs of the PEP-II Positron Ring*, LBNL Report LBNL-441123/CBP Notes-246, PEP-II AP Note AP 97.27, Proc. Int. Workshop on Multibunch Instabilities in Future Electron and Positron Accelerators (MBI-97), ed. Y.H. Chin, KEK, Tsukuba, Japan, July 15–18, 1997; M. A. Furman, *The Electron-Cloud Effect in the Arcs of the LHC*, LBNL Report LBNL-41482/CBP Note 247/LHC Project Report 180, May 20, 1998.
- [3] This is derived assuming uniform transverse distribution in the electron cloud. See for example, M.A. Furman, *A Preliminary Assessment of the Electron Cloud Effect for the FNAL Main Injector*, LBNL Report LBNL-57634/CBP-Note-712, 2006.
- [4] S. Heifets, Wake field of the e-cloud, Proc. 23rd Advanced ICFA Beam Dynamics Workshop on High Luminosity e^+e^- Collider, Ithaca, NY, October 15-19, 2001; SLAC-PUB-9025, 2001.
- [5] K.Y. Ng, *Analysis of Possible Electron-Cloud Induced Collective Instabilities in the Fermilab Booster*, Fermilab Report FERMILAB-FN-0806-AD, 2007.
- [6] K.Y. Ng, *Coupling Impedances of Laminated Magnets*, Fermilab Report FN-0744, 2004.
- [7] K.Y. Ng, *Electron Cloud in the Fermilab Booster*, Proceedings of U.S. Particle Accelerator Conference (PAC'07), Albuquerque, NM, June 25–29, 2007, p. 3895.
- [8] See for example, K. Y.Ng, *Distribution of Incoherent Space-Charge Tune Shift of a Bi-Gaussian Beam*, Fermilab Report TM-2241, 2004.
- [9] Xiaobiao Huang, *Beam Diagnosis and Lattice Modeling of the Fermilab Booster*, PhD thesis, Indiana University, 2005; X. Huang, *The Coherent Detuning of Vertical Betatron Tunes*, 2005, unpublished; X. Huang, S. Y. Lee, E. Prebys, and R. Tomlin, *Application of independent component analysis to Fermilab Booster*, *Phys. Rev. ST Accel. Beams* **8**, 064001 (2005).
- [10] X. Huang, *Bunch Length Measurements at Different Intensity*, 2005, unpublished.

- [11] See for example, *Handbook of Accelerator Physics and Engineering*, Ed. A.W. Chao and M. Tigner, 3rd Printing, 2006, p.130.
- [12] K.Y. Ng, *Impedances and Collective Instabilities of the Tevatron at Run II*, Fermilab Report TM-2055, 1998.